On the role of conical intersections and their local topography in the photodissociation of the 1-hydroxyethyl radical

ARTICLE *in* CHEMICAL PHYSICS · DECEMBER 2010

Impact Factor: 1.65 · DOI: 10.1016/j.chemphys.2010.10.011

2 AUTHORS, INCLUDING:

Kousik Samanta

Indian Institute of Technology Bhubaneswar

9 PUBLICATIONS **112** CITATIONS

SEE PROFILE

Chemical Physics 378 (2010) 110–117

Contents lists available at ScienceDirect

Chemical Physics

journal homepage: www.elsevier.com/locate/chemphys

On the role of conical intersections and their local topography in the photodissociation of the 1-hydroxyethyl radical

Kousik Samanta [1], David R. Yarkony *

Department of Chemistry, Johns Hopkins University, Baltimore, MD 21218, USA

ARTICLE INFO

Article history:
Received 18 August 2010
In final form 20 October 2010
Available online 25 October 2010

Keywords:
Conical intersection
CH_3CHOH
1-Hydroxyethyl radical
Photodissociation
Rydberg states

ABSTRACT

The role of conical intersections in the photodissociation of the 1-hydroxyethyl radical is investigated. Two local minima on the 1^2A–2^2A seam of the conical intersection, which correspond to significant stretching of either the O–H or the nonmethyl C–H bond are located, as is an energy minimized intersection on the 2^2A–3^2A seam. The local topography for these conical intersections is determined from the average energy gradient, energy difference gradient and interstate coupling gradient and used to discuss the mechanism of photodissociation. The results are compared with a theoretical study of the hydroxymethyl radical, and are used to explain recent REMPI and photofragment yield spectra. The absence of a REMPI spectrum for the 2^2A state, nominally the 3s Rydberg state, is attributed to a 1^2A–2^2A conical intersection. Time-of-flight spectra in the region of the 2^2A state are discussed, as are spectra in the region of the 3^2A, a 3p Rydberg, state.

1. Introduction

Hydroxyalkyl radicals play important roles as reaction intermediates in atmospheric and combustion chemistry [1–7]. A recent study of aldehyde-enol tautomerism of ethanal and ethanol in the flames of ethanol, olefins and commercial fluids establishes the significance of the 1-hydroxyethyl radical (CH_3CHOH) as a combustion intermediate [8]. CH_3CHOH and its isomer CH_2CH_2OH (2-hydroxyethyl) were found to be relevant to the photochemistry of ethoxy radicals as well [9].

Recently Karpichev et al. [10] (denoted KEWR below) studied the photochemistry of 1-hydroxyethyl, using resonance enhanced multiphoton ionization (REMPI) and photofragment yield spectroscopy. These results complemented earlier experimental studies of the hydroxymethyl radical (CH_2OH) [11–16] which had also been the subject of several computational studies [17–23]. To understand the results of KEWR's experiments on 1-hydroxyethyl, and our calculations that follow in Section 3, several observations are relevant. In the ground, 1^2A state of 1-hydroxyethyl, the singly occupied molecular orbital (SOMO) is largely a π^* orbital perpendicular to the $C^{(2)}$–$C^{(1)}$–$H^{(2)}$ plane. See Fig. 1 for atom numbering used in this work. The low-lying electronic states 2^2A–5^2A result from excitations from the π^* SOMO to the (largely carbon) 3s and $3p_x$, $3p_y$, $3p_z$ Rydberg orbitals. Using a quantum defect model based on previous results for hydroxymethyl, KEWR estimated the energies of the 3s, $3p_x$ and $3p_z$ Rydberg states of CH_3CHOH to be 18,527 (25,971), 27,695 (35,004) and 33,684 (41,053) cm^{-1}, where the energies of CH_2OH are given in parentheses. The significant differences in the excitation energies between hydroxymethyl and 1-hydroxyethyl are a consequence of the dramatically lower ionization energy of 1-hydroxyethyl when compared with hydroxymethyl. Krylov and coworkers [24] have attributed this to hyperconjugation in 1-hydroxyethyl. Since the 1-hydroxyethyl cation is bound [24] (as is the hydroxymethyl cation [25]) these Rydberg states are expected to be bound. However it is known that in hydroxymethyl, owing to conical intersections of the 1^2A–2^2A states, the 2^2A state, the 3s Rydberg state, is dissociative [13,14,20] on a sufficiently short time scale to preclude REMPI detection [14]. Measurements by KEWR indicate a similar situation in 1-hydroxyethyl, where again no REMPI signal was obtained in the spectral region where their estimates indicated the 2^2A state should be found. This has implications for the spectra of the remaining Rydberg states, as coupling of the 2^2A and n^2A states, $n > 2$ can result in lifetime broadening and predissociation of the higher electronic states. Photofragment yield spectroscopy provides information regarding electronic states not visible by REMPI. With regard to potential dissociation products, the channels with the lowest dissociation energies for CH_3CHOH are determined from theoretical calculations to be [26]

$$CH_3CHOH \rightarrow CH_3CHO + H, \quad \Delta H = 1.04\,eV \ (8389\,cm^{-1}) \tag{1a}$$
$$CH_3CHOH \rightarrow H + CH_2CHOH, \quad \Delta H = 1.46\,eV \ (11{,}776\,cm^{-1}) \tag{1b}$$
$$CH_3CHOH \rightarrow CH_3 + CHOH, \quad \Delta H = 3.13\,eV \ (25{,}246\,cm^{-1}) \tag{1c}$$
$$CH_3CHOH \rightarrow CH_3COH + H, \quad \Delta H = 3.37\,eV \ (27{,}182\,cm^{-1}) \tag{1d}$$

* Corresponding author.
E-mail address: yarkony@jhu.edu (D.R. Yarkony).
[1] Present address: Department of Chemistry, Rice University, Houston, TX, USA.

0301-0104/$ - see front matter © 2010 Elsevier B.V. All rights reserved.
doi:10.1016/j.chemphys.2010.10.011

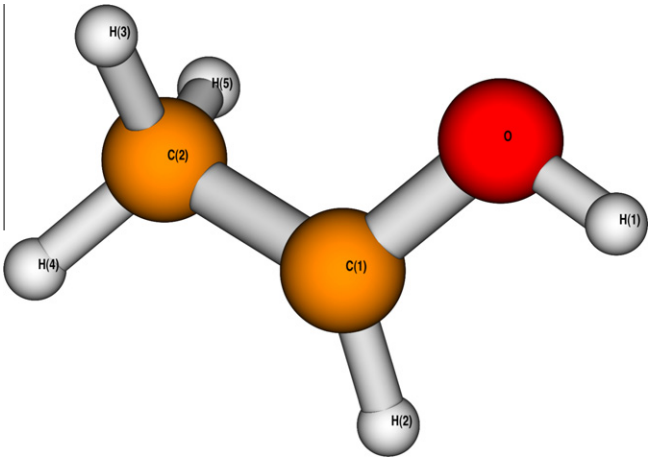

Fig. 1. Ball and stick representation of 1-hydroxyethyl.

with ΔH being the thermochemical dissociation threshold. KEWR reported the onset of the H fragment signal at $19600 \pm 100\ cm^{-1}$ from the photofragment yield spectra and assigned it to absorption to the 2^2A state, the 3s Rydberg state, on the basis of the above estimates of the Rydberg state energies. However, they could not assign any absorption to $3p_x$ Rydberg state as the photofragment yield spectrum near their estimated excitation energy of $27{,}695\ cm^{-1}$ did not reveal any feature that could distinguish it from the absorption to the 3s state. Further, no REMPI signal was observed in this region until $\sim 32{,}000\ cm^{-1}$, the origin band of what their estimates indicate is the $3p_z$ state, leading them to conclude that the $3p_x$ state of CH_3CHOH is predissociated. Within this spectral region, 32,000–$38{,}000\ cm^{-1}$, they observed a "structured" 2 + 2 REMPI spectrum with the peaks separated by $1560 \pm 100\ cm^{-1}$. These peaks were attributed to a vibrational progression in the C–O stretch excitation. They assigned the center of the lowest energy peak, at $32{,}360 \pm 70\ cm^{-1}$, to the origin band of the transition to the $3p_z$ Rydberg state based on their estimated onset at $33{,}684\ cm^{-1}$. The time-of-flight of the photofragment spectrum recorded after $21{,}212\ cm^{-1}$ excitation showed a single peak with strong negative recoil anisotropy. However excitation at 31,250 and $35{,}460\ cm^{-1}$ showed two peaks, one with a very low negative anisotropy indicating statistical redistribution of available energy among the internal modes.

The work of KEWR demonstrates the significant impact of nonadiabatic interactions on the recorded spectra of 1-hydroxyethyl. Here we report computational studies aimed at understanding the origin of these nonadiabatic effects. We are particularly interested in the location and local topography of conical intersections and how they could impact the observed spectra. The local topography will be deduced from the average energy gradient **s**, the energy difference gradient **g** and the interstate coupling gradient **h**. Although previous computational studies of CH_3CHOH have been reported [24,26,27], there are no previous computational studies addressing these issues. We will describe our computational methods in Section 2, and report and discuss our results in Section 3. Section 4 concludes our discussion and indicates future research directions.

2. Theoretical approach

All the *ab initio* electronic structure calculations were performed at the multi-reference configuration interaction with single and double excitations (MRCISD) level. The molecular orbitals for the MRCISD calculations were obtained from the state-averaged restricted active space self-consistent field (SA-RASSCF) calculations. All calculations were performed using the COLUMBUS suite of electronic structure codes [28–30].

2.1. Basis set

For each of the heavy atoms, C and O, a 7s6p2d1f basis set was used. This was obtained by augmenting Dunning's correlation-consistent polarized valence triple-ζ basis set, cc-pVTZ (4s3p 2d1f), [31] with three uncontracted diffuse s- and p-type functions whose exponents are in geometric progression [32] with those of the two most diffuse *s* and *p* functions in the original cc-pVTZ basis set. These additional basis functions were included to describe the Rydberg states. Dunning's double-ζ polarized basis set, DZP (2s1p), [33] was used for each of the hydrogen atoms. These resulted in a total of 151 contracted Gaussian-type basis functions for the current calculation.

2.2. SA-RASSCF molecular orbitals

The computed wave functions must be able to describe significant elongation of the O–H, methyl C–H and non-methyl C–H bonds, in both the ground and low-lying excited states, and the electronic reorganization of the incipient singlet diradical (which ultimately becomes a closed shell species) on the residual (CH_2CHOH, CH_3COH, or CH_3CHO) moiety. Here C–C bond fission is not considered. Ideally this description would be accomplished by treating all C–H and O–H bonds equivalently, that is, including $\sigma(\mathrm{C{-}H}),\ \sigma*(\mathrm{C{-}H}), \sigma(\mathrm{O-H}),\ \sigma^*(\mathrm{O{-}H})$ orbitals together with valence and Rydberg SOMOs in a complete active space (CAS), reference space calculation. However an MRCISD calculation based on that active space would be prohibitively expensive. Instead we use the restricted active space (RAS) method to approximate the CAS as a sum of direct products of distinct distributions of electrons in two RAS spaces, *ras1* and *ras2*. The *ras1* subspace is composed of four orbitals, two bonding and antibonding orbital pairs which can describe elongation of $O{-}H^{(1)}$ and either $C^{(1)}{-}H^{(2)}$ or $C^{(2)}{-}H^{(4)}$ bonds (see Fig. 1 for numbering), whereas *ras2* was composed of the valence space SOMO, and three Rydberg-type orbitals (an s and two p type orbitals). Depending on the choice of $C^{(2)}{-}H^{(4)}$ or $C^{(1)}{-}H^{(2)}$ bonding-antibonding pairs in *ras1*, the calculation was termed the "methyl" or "non-methyl" case. The "methyl" and "non-methyl" results are local solutions to the state-averaged multiconfiguration self-consistent field problem. It will emerge that the inclusion of σ^* orbitals in the active space is essential for the description of conical intersections with the corresponding bond stretched. The "methyl" *ras1* does not treat all three methyl hydrogens equivalently. This will introduce small errors in the description of the methyl group which will be seen to be inconsequential for the issues being addressed in this work. However, when the "non-methyl" results are appropriate they are preferred. The *ras2* subspace was restricted to house at most one electron, and accordingly *ras1* might house four or five electrons so that the total number of electrons in these two subspaces was always five. All the calculations were performed without any spatial symmetry restriction.

In order to obtain a set of molecular orbitals suitable for describing the ground as well as the excited states, the average energy of the four lowest states with equal weights was minimized using a RASSCF procedure. The molecular orbitals obtained from these state-averaged RASSCF (SA-RASSCF) calculations were used for the MRCISD calculations.

2.3. MRCISD wavefunctions

In the MRCISD expansion, the *1s* orbitals on C and O atoms were kept frozen (i.e., they were always kept doubly occupied and no

excitations were allowed from them) and seven molecular orbitals with 14 electrons were included in a doubly occupied space, *dos*. From the *dos* single and double excitations were allowed. All possible single and double excitations were allowed to and from the *ras1* while the *ras2* subspace was treated as an auxiliary subspace (*aux*). In this case the *aux* space was restricted to have one electron at most. Finally, the generalized interacting space restrictions were imposed for all MRCISD calculations. The resulting MRCISD space was comprised of 104,125,400 configuration state functions (CSFs) of doublet spin symmetry. The three lowest energy electronic states, nominally the ground state, the 3s and $3p_x$ Rydberg states, will be treated at this level. The accuracy of this description will be evaluated in Section 3.

3. Results and discussion

In this work a geometry $\mathbf{Q}$ is expressed in terms of 18 internal coordinates $\mathbf{Q} = [R_{C^{(1)}O}, R_{C^{(1)}C^{(2)}}, R_{OH^{(1)}}, R_{C^{(1)}H^{(2)}}, R_{C^{(2)}H^{(3)}}, R_{C^{(2)}H^{(4)}}, R_{C^{(2)}H^{(5)}}, \theta_{C^{(2)}C^{(1)}O}, \theta_{H^{(1)}OC^{(1)}}, \theta_{H^{(2)}C^{(1)}O}, \theta_{H^{(3)}C^{(2)}C^{(1)}}, \theta_{H^{(4)}C^{(2)}C^{(1)}}, \theta_{H^{(5)}C^{(2)}C^{(1)}}, \gamma_{H^{(1)}OC^{(1)}C^{(2)}}, \gamma_{H^{(2)}C^{(1)}OH^{(1)}}, \gamma_{H^{(3)}C^{(2)}C^{(1)}O}, \gamma_{H^{(4)}C^{(2)}C^{(1)}O}, \gamma_{H^{(5)}C^{(2)}C^{(1)}O}]$ where R_{AB} is the distance between atoms A and B in Å, θ_{ABC} is the angle between the line segments AB and BC in degrees, and γ_{ABCD} is the dihedral angle between the planes ABC and BCD in degrees. $\tilde{E}_J(\mathbf{Q})$ is the energy of state J^2A, in a.u. with the geometry $\mathbf{Q}$. $E_J(\mathbf{Q}) = \tilde{E}_J(\mathbf{Q}) - \tilde{E}_1(\mathbf{Q}_1^{\min})$ is given in wave numbers where $\mathbf{Q}_1^{\min}$ is the ground state equilibrium geometry.

We began by looking for the minimum energy structures on the three lowest potential energy surfaces, denoted $\mathbf{Q}_J^{\min}$ $J = 1$–3 and energy minimized conical intersections that couple those states, conical intersections of the 1^2A and 2^2A states, and of the 2^2A and 3^2A states, denoted $\mathbf{Q}_{I,J}^{\text{mex,B}}$, where I^2A, J^2A denote the states and B is an attribute described below. The results of these calculations are reported in Table 1 which compares the total energies, in a.u., obtained for the "methyl" and "non-methyl" *ras1* calculations; Table 2 which reports the geometries of the determined minima; Table 3 which reports the geometries of the determined energy minimized conical intersections; and Table 4 which reports the relative energetics for all computed extrema. These tables are of interest both for what is reported and what was not found. The cartesian geometries for all these structure are reported in the supplemental data [34], as are ball and stick representations of these structures.

Firstly note that largely equivalent results were obtained for the "methyl" and "non-methyl" *ras1* subspaces. The total energies reported in Table 1 differ by less than 4 mh. These differences in the total energies result, as can be seen from Table 4, in relative energies which differ by at most 3%. As seen in Tables 2 and 3 the determined structures are largely equivalent, except for some not unexpected differences in the dihedral angles which reflect comparatively low-energy reorientations of the methyl group. As noted above the "non-methyl" *ras1* based results are preferred when applicable, which will turn out to include all calculations reported in these tables. Consequently in the discussions that follow, "non-methyl" results are quoted unless otherwise indicated. There is however one notable difference, which is discussed and explained in section IIIBi below.

Table 1
Total energies in hartrees at extrema on the three lowest PESs. In the final column CH refers to $C^{(1)}H^{(2)}$.

Energy	$\mathbf{Q}_1^{\min}$	$\mathbf{Q}_3^{\min}$	$\mathbf{Q}_{1,2}^{\text{mex,OH}}$	$\mathbf{Q}_{2,3}^{\text{mex}}$	$\mathbf{Q}_{1,2}^{\text{mex,CH}}$
Non-methyl					
$\tilde{E}_1(\mathbf{Q})$	−154.037246	−154.018690	−153.951791	−153.983715	−153.907741
$\tilde{E}_2(\mathbf{Q})$	−153.902761	−153.938075	−153.951791	−153.880042	−153.907741
$\tilde{E}_3(\mathbf{Q})$	−153.869091	−153.899304	−153.846874	−153.880042	−153.788512
Methyl					
$\tilde{E}_1(\mathbf{Q})$	−154.034398	−154.016152	−153.950060	−153.979806	
$\tilde{E}_2(\mathbf{Q})$	−153.903094	−153.937977	−153.950060	−153.877824	
$\tilde{E}_3(\mathbf{Q})$	−153.869413	−153.899157	−153.842126	−153.877824	

Table 2
$\mathbf{Q}_1^{\min}$, $\mathbf{Q}_3^{\min}$. Here m (nm) denotes the "methyl"("non-methyl") case. For hydroxymethyl at $\mathbf{Q}_1^{\min}$ (from Ref. [22]) $R_{CO} = 1.376$, $R_{OH} = 0.965$, $\bar{R}_{CH} = 1.073$ Å and $\mathbf{Q}_3^{\min}$ (from Ref. [20]) $R_{CO} = 1.264$, $R_{OH} = 0.989$, $\bar{R}_{CH} \sim 1.102$ Å. Here $\bar{R}_{CH}$ is the average of the two CH bond lengths in hydroxymethyl.

	$\mathbf{Q}_1^{\min}$ (m)	$\mathbf{Q}_1^{\min}$ (nm)	$\mathbf{Q}_1^{\min}$ (Ref. [24])	$\mathbf{Q}_3^{\min}$ (m)	$\mathbf{Q}_3^{\min}$ (nm)	*Ion* (Ref. [24])
$R_{C^{(1)}O}$	1.362	1.363	1.373	1.259	1.259	1.262
$R_{C^{(1)}C^{(2)}}$	1.477	1.479	1.476	1.448	1.450	1.445
$R_{OH^{(1)}}$	0.961	0.961	0.959	0.983	0.983	0.975
$R_{C^{(1)}H^{(2)}}$	1.077	1.090	1.078	1.088	1.098	1.083
$R_{C^{(2)}H^{(3)}}$	1.086	1.092	1.084	1.084	1.093	1.091
$R_{C^{(2)}H^{(4)}}$	1.094	1.086	1.092	1.102	1.083	1.081
$R_{C^{(2)}H^{(5)}}$	1.093	1.085	1.086	1.092	1.092	1.091
$\theta_{C^{(2)}C^{(1)}O}$	113.9	113.9	114.0	119.4	119.5	120.0
$\theta_{H^{(1)}OC^{(1)}}$	109.1	109.1	108.3	114.4	114.5	113.9
$\theta_{H^{(2)}C^{(1)}O}$	116.6	116.4		119.8	120.0	
$\theta_{H^{(3)}C^{(2)}C^{(1)}}$	110.7	111.8		112.7	107.3	
$\theta_{H^{(4)}C^{(2)}C^{(1)}}$	110.3	110.5		106.9	112.5	
$\theta_{H^{(5)}C^{(2)}C^{(1)}}$	111.9	111.2		107.6	107.4	
$\gamma_{H^{(1)}OC^{(1)}C^{(2)}}$	175.3	175.5	−175.1	−179.9	−179.9	180.0
$\gamma_{H^{(2)}C^{(1)}OH^{(1)}}$	27.6	28.4		−0.1	0.0	
$\gamma_{H^{(3)}C^{(2)}C^{(1)}O}$	53.0	−53.4	−52.0	−0.6	0.3	−0.1
$\gamma_{H^{(4)}C^{(2)}C^{(1)}O}$	172.8	66.2	66.7	123.5	124.1	123.2
$\gamma_{H^{(5)}C^{(2)}C^{(1)}O}$	−67.1	−173.5	−171.8	−125.9	−125.0	−123.4

Table 3
$\mathbf{Q}_{1,2}^{mex,OH}$, $\mathbf{Q}_{1,2}^{mex,CH}$. Here m (nm) denotes the "methyl"("non-methyl") case. For 1-hydroxyethyl, $\mathbf{Q}_{1,2}^{mex,CH} = \mathbf{Q}_{1,2}^{mex,C^{(1)}H^{(2)}}$. For hydroxymethyl, at $\mathbf{Q}_{1,2}^{mex,OH}$, $R_{CO} = 1.235$, $R_{OH} = 1.375$, $\bar{R}_{CH} \sim 1.084$ Å (Ref. [22]). Here $\bar{R}_{CH}$ is the average of the two CH bond lengths in hydroxymethyl. At an approximate $\mathbf{Q}_{2,3}^{mex,CH}$ for hydroxymethyl $R_{CO} = 1.291$, $R_{OH} = 0.977$, $R_{CH} = 1.397$ Å (Ref. [20]).

	$\mathbf{Q}_{1,2}^{mex,OH}$ (nm)	$\mathbf{Q}_{1,2}^{mex,OH}$ (m)	$\mathbf{Q}_{1,2}^{mex,CH}$ (nm)	$\mathbf{Q}_{2,3}^{mex}$ (nm)	$\mathbf{Q}_{2,3}^{mex}$ (m)
$R_{C^{(1)}O}$	1.231	1.231	1.277	1.301	1.311
$R_{C^{(1)}C^{(2)}}$	1.485	1.486	1.480	1.487	1.487
$R_{OH^{(1)}}$	1.343	1.346	0.972	0.974	0.973
$R_{C^{(1)}H^{(2)}}$	1.102	1.091	1.765	1.287	1.275
$R_{C^{(2)}H^{(3)}}$	1.088	1.087	1.092	1.089	1.082
$R_{C^{(2)}H^{(4)}}$	1.084	1.093	1.091	1.082	1.099
$R_{C^{(2)}H^{(5)}}$	1.086	1.087	1.089	1.088	1.085
$\theta_{C^{(2)}C^{(1)}O}$	122.4	121.4	110.6	109.7	108.6
$\theta_{H^{(1)}OC^{(1)}}$	106.9	106.7	106.3	110.8	110.8
$\theta_{H^{(2)}C^{(1)}O}$	118.2	118.3	97.2	150.2	149.2
$\theta_{H^{(3)}C^{(2)}C^{(1)}}$	108.4	109.9	113.8	107.1	112.1
$\theta_{H^{(4)}C^{(2)}C^{(1)}}$	110.9	111.1	106.1	113.5	106.8
$\theta_{H^{(5)}C^{(2)}C^{(1)}}$	111.0	109.9	111.1	107.5	110.4
$\gamma_{H^{(1)}OC^{(1)}C^{(2)}}$	178.5	180.0	176.1	−179.8	−173.1
$\gamma_{H^{(2)}C^{(1)}OH^{(1)}}$	−0.5	0.0	−1.7	−0.1	8.5
$\gamma_{H^{(3)}C^{(2)}C^{(1)}O}$	−29.8	59.1	−95.3	−0.1	−3.4
$\gamma_{H^{(4)}C^{(2)}C^{(1)}O}$	88.5	−180.0	23.6	123.0	116.8
$\gamma_{H^{(5)}C^{(2)}C^{(1)}O}$	−152.8	−59.0	149.5	−124.0	−128.9

Table 4
Energetics of extrema. Here m (nm) denotes the "methyl"("non-methyl") case. $\mathbf{Q}_{1,2}^{mex,CH} = \mathbf{Q}_{1,2}^{mex,C^{(1)}H^{(2)}}$. The energy at $\mathbf{Q}_{1,2}^{mex,OH}$ for hydroxymethyl is 19,737 cm^{-1}[22]. The energies for hydroxymethyl at $\mathbf{Q}_3^{min}$ and at an approximate $\mathbf{Q}_{2,3}^{mex}$ are 33,587 and 37,772 cm^{-1}, [20] respectively.

	$\mathbf{Q}_1^{min}$ (nm)	$\mathbf{Q}_1^{min}$ (m)	$\mathbf{Q}_3^{min}$ (nm)	$\mathbf{Q}_3^{min}$ (m)	$\mathbf{Q}_{1,2}^{mex,OH}$ (nm)	$\mathbf{Q}_{1,2}^{mex,OH}$ (m)	$\mathbf{Q}_{1,2}^{mex,CH}$ (nm)	$\mathbf{Q}_{2,3}^{mex}$ (nm)	$\mathbf{Q}_{2,3}^{mex}$ (m)
$E_1(\mathbf{Q})$	0	0	4073	4005	18,661	18,510	28,422	11,749	11,981
$E_2\mathbf{Q})$	29,516	28,818	21,766	21,162	18,661	18,510	28,422	34,502	34,360
$E_3\mathbf{Q})$	36,906	36,210	30,275	29,682	41,782	42,199	54 591	34,502	34,360

3.1. Equilibrium structures

The ground state equilibrium structure for 1-hydroxyethyl is reported in Table 2 for the "methyl" and "non-methyl" *ras1* spaces and compared with a previous CCSD(T)/cc-pVTZ calculation by Krylov and coworkers [24]. The CCSD(T) method is expected to give very reliable equilibrium structures. Therefore the good agreement with the CCSD(T) results for the $\mathbf{Q}_1^{min}$ in Table 2 which for the "non-methyl" case includes the orientation of the methyl group, is reassuring. The geometrical comparison with the CCSD(T) results in Table 2 involving $\mathbf{Q}_3^{min}$ which again for the "non-methyl" case include the orientation of the methyl, is also very good. Note, for example, that the large decrease in $R_{C^{(1)}O}$ (∼0.1 Å) in going from $\mathbf{Q}_1^{min}$ to $\mathbf{Q}_3^{min}$ is well reproduced. However in this case we are not comparing two calculations of $\mathbf{Q}_3^{min}$, but rather our determination of $\mathbf{Q}_3^{min}$ with the ground state equilibrium structure of the 1-hydroxyethyl *cation*. This reflects, and confirms, the anticipated 3p Rydberg + ion core character of the 3^2A state near its equilibrium structure. Note that the $C^{(1)}O$ and $OH^{(1)}$ bond distances for $\mathbf{Q}_1^{min}$ and $\mathbf{Q}_3^{min}$ are in good accord with those previously obtained for hydroxymethyl [20,22] which are collected in Table 2. $\mathbf{Q}_3^{min}$ lies 30,275 (29,682) cm^{-1} above the ground state minimum for the "non-methyl" ("methyl") case. This separation is significantly larger than the estimate of 27,695 cm^{-1} of KEWR, which was based on comparison with hydroxymethyl results. It is also worth noting that for $\mathbf{Q}_3^{min}$ a largely CO stretch mode with frequency 1680 cm^{-1} was found.

Notable for its absence from Table 2, is $\mathbf{Q}_2^{min}$, the equilibrium structure for the 2^2A or 3s Rydberg state. All attempts to optimize this structure failed. This is precisely the same situation as we found in hydroxymethyl, where minima were found for the 1^2A and 3^2A states, but not for the 2^2A state [20]. The absence of a local minimum on the 2^2A potential energy surface is caused by a conical intersection of states 1^2A and 2^2A, denoted $\mathbf{Q}_{1,2}^{mex,OH}$ below, to which we now turn.

3.2. Conical Intersections

3.2.1. Location

Conical intersections were shown to have an enormous impact on the REMPI and photofragment yield spectra of hydroxymethyl. In 1- hydroxyethyl, the failure of KEWR to observe REMPI signals in regions where Rydberg states were expected suggests the existence of similar nonadiabatic effects. Tables 3 and 4 address this issue.

We begin with conical intersections connecting the ground and first excited states with locations $\mathbf{Q}_{1,2}^{mex,A}$, with the attribute A = OH, $C^{(1)}H^{(2)}$ and $C^{(2)}H^{(4)}$ indicating the extension of the corresponding bond. Firstly note that a conical intersection with $R_{OH^{(1)}}$ stretched from 0.983 Å at $\mathbf{Q}_1^{min}$ to ∼1.345 Å at $\mathbf{Q}_{1,2}^{mex,A}$ was found. This energy minimized conical intersection, is 18,510 (18,661) cm^{-1} above $\mathbf{Q}_1^{min}$ using the "non-methyl" ("methyl") *ras1*. Again the $OH^{(1)}$ and $C^{(1)}O$ bond lengths at $\mathbf{Q}_{1,2}^{mex,OH}$ are similar to those found in hydroxymethyl as can be seen in Table 3.

An additional energy minimized conical intersection, $\mathbf{Q}_{1,2}^{mex,C^{(1)}H^{(2)}}$ was located and is reported in Table 3. In this structure, $R_{C^{(1)}H^{(2)}}$ increases from 1.098 Å for $\mathbf{Q}_3^{min}$ to 1.765 Å for $\mathbf{Q}_{1,2}^{mex,C^{(1)}H^{(2)}}$. Energetically it is 28,477 cm^{-1} above $E_1(\mathbf{Q}_1^{min})$ and ∼9600 cm^{-1} above $E_1(\mathbf{Q}_{1,2}^{mex,OH})$ The long $R_{C^{(1)}H^{(2)}}$ bond puts this conical intersection only 1353 cm^{-1} above the $CH_3COH + H$ asymptote, calculated to be at 27,124 cm^{-1} (3.362 eV) relative to $E_1(\mathbf{Q}_1^{min})$. This predicted dissociation energy is in good accord with that obtained in a previous theoretical study [10,26]. See channel (1d) in the Introduction. Given

the long $C^{(1)}$–$H^{(2)}$ bond it is not surprising that this conical intersection was only found using the "non-methyl" *ras1*.

Comparing this result with our previous study of hydroxymethyl photodissociation suggests that additional conical intersections of this type could be found for shorter $C^{(1)}$–$H^{(2)}$ bond distances [22]. However it will emerge that this issue is not germane to our analysis of the KEWR measurements, and therefore will be deferred to a future study.

Searches were performed to locate conical intersections with the $C^{(2)}$–$H^{(4)}$ bond stretched using the "methyl" *ras1*. However these searches were unsuccessful. For this reason and to save writing, the $\mathbf{Q}^{\mathrm{mex},C^{(1)}H^{(2)}}_{1,2}$ conical intersection is subsequently denoted $\mathbf{Q}^{\mathrm{mex,CH}}_{1,2}$, when no confusion will result.

Next we turn to the possibility of conical intersections that can connect the 2^2A and 3^2A states, that is those that impact the stability of the 3^2A state. The minimum energy conical intersection for these states (approximately equivalent results were obtained for both the "methyl" and "non-methyl" *ras1* subspace), $\mathbf{Q}^{\mathrm{mex}}_{2,3}$, is reported in Table 3. The principal difference between $\mathbf{Q}^{\mathrm{mex}}_{2,3}$ and $\mathbf{Q}^{\mathrm{min}}_{3}$ is ~0.2 Å increase in $R_{C^{(1)}H^{(2)}}$. From Table 4 the energy of this conical intersection was found to be approximately 4227 cm^{-1} above $E_3(\mathbf{Q}^{\mathrm{min}}_3)$. The $C^{(1)}O$ and $OH^{(1)}$ bond distances at $\mathbf{Q}^{\mathrm{mex}}_{2,3}$ are similar to those reported in a previous study of hydroxymethyl. See Table 3. However the stretched CH bond, $R_{C^{(1)}H^{(2)}}$ is ~0.1 Å shorter in 1-hydroxyethyl than in hydroxymethyl. It should be noted in this regard that $R_{C^{(1)}H^{(2)}}$ was fixed in the hydroxymethyl calculation rather than optimized as in the present calculations. On the other hand for the partially optimized $\mathbf{Q}^{\mathrm{mex}}_{2,3}$ in hydroxymethyl, $E_3(\mathbf{Q}^{\mathrm{mex}}_{2,3}) - E_3(\mathbf{Q}^{\mathrm{min}}_3) \sim +4186\ \mathrm{cm}^{-1}$ consistent with the ~4227 cm^{-1} in 1-hydroxyethyl noted above.

3.3. Topography of conical intersections

A photochemically excited electronic state may be funneled to a lower state in a radiationless fashion through a conical intersection between the two states. The local topography of the conical intersection influences the both the efficacy and outcome of that process. In this section we use the average energy gradient $\mathbf{s}^{IJ}$, the energy difference gradient $\mathbf{g}^{IJ}$ and the interstate coupling gradient, $\mathbf{h}^{IJ}$ for states I^2A, J^2A to describe the local topography of the conical intersections reported in Section 3.2.1 above. Below we review the relevant ideas.

Near a point of conical intersection $(\mathbf{Q}^x_{IJ})$

$$E_{\pm}(\mathbf{Q}) = E_I(\mathbf{Q}^x_{IJ}) + (s^{IJ}_x x + s^{IJ}_y y) \pm [(g^{IJ}x)^2 + (h^{IJ}y)^2]^{1/2} \tag{1a}$$

where

$$\mathbf{Q} = \mathbf{Q}^x_{IJ} + \hat{\mathbf{x}}x + \hat{\mathbf{y}}y \tag{1b}$$

and

$$\hat{\mathbf{x}} = \mathbf{g}^{IJ}/g^{IJ}; \quad g^{IJ} = ||\mathbf{g}^{IJ}||; \quad \hat{\mathbf{y}} = \mathbf{h}^{IJ}/h^{IJ}; \quad h^{IJ} = ||\mathbf{h}^{IJ}|| \tag{2a}$$

$$s^{IJ}_x = \mathbf{s}^{IJ}\cdot\hat{\mathbf{x}} \quad \text{and} \quad s^{IJ}_y = \mathbf{s}^{IJ}\cdot\hat{\mathbf{y}} \tag{2b}$$

The asymmetry and pitch are defined by

$$\Delta^{IJ} = (g^{IJ^2} - h^{IJ^2})/(g^{IJ^2} + h^{IJ^2}) \text{ and } p^{IJ} = (g^{IJ^2} + h^{IJ^2})^{1/2} \tag{3}$$

respectively. The significance of these parameters is discussed below. See also Ref. [35].

It is convenient to define polar coordinates $x = \rho\cos\theta$ and $y = \rho\sin\theta$. In that case the singular part of the derivative coupling is given by $(1/\rho)/f^{IJ}_\theta$, where [36]

$$f^{IJ}_\theta \equiv 0.5\frac{g^{IJ}h^{IJ}}{(g^{IJ^2}\cos^2\theta + h^{IJ^2}\sin^2\theta)} \tag{4}$$

The $\mathbf{s}^{IJ}$, $\mathbf{g}^{IJ}$ and $\mathbf{h}^{IJ}$ are determined from the solutions of electronic Schrödinger equation

$$(\mathbf{H}^{\mathrm{CSF}}(\mathbf{Q}) - E_I(\mathbf{Q})\mathbf{I})\mathbf{c}^I(\mathbf{Q}) = \mathbf{0} \tag{5}$$

as follows:

$$\mathbf{h}^{IJ}(\mathbf{Q}) = \mathbf{c}^I(\mathbf{Q})^\dagger\nabla\mathbf{H}^{\mathrm{CSF}}(\mathbf{Q})\mathbf{c}^J(\mathbf{Q}); \quad \mathbf{g}^{IJ} = (\mathbf{h}^{I,I} - \mathbf{h}^{J,J})/2;$$
$$s^{IJ} = (\mathbf{h}^{I,I} + \mathbf{h}^{J,J})/2 \tag{6}$$

where $\mathbf{H}^{\mathrm{CSF}}$ is the electronic Hamiltonian in the CSF basis.

The $\mathbf{g}^{IJ}$ and $\mathbf{h}^{IJ}$ vectors at $\mathbf{Q}^{\mathrm{mex,OH}}_{1,2}$, $\mathbf{Q}^{\mathrm{mex,CH}}_{1,2}$ and $\mathbf{Q}^{\mathrm{mex}}_{2,3}$ are pictured in Figs. 2–4. The characteristic parameters, s^{IJ}_x, s^{IJ}_y, g^{IJ}, h^{IJ}, p^{IJ} and Δ^{IJ} are given in Table 5. Approximately the same results are obtained for "methyl" and "non-methyl" *ras*1 for $\mathbf{Q}^{\mathrm{mex,OH}}_{1,2}$ and $\mathbf{Q}^{\mathrm{mex}}_{2,3}$. We focus our attention on the conical intersections at $\mathbf{Q}^{\mathrm{mex,OH}}_{1,2}$ and $\mathbf{Q}^{\mathrm{mex}}_{2,3}$. The pitch of the double cone at $\mathbf{Q}^{\mathrm{mex,OH}}_{1,2}$ is about 2.5 times as big as that for $\mathbf{Q}^{\mathrm{mex}}_{2,3}$, which is indicative of more efficient transfer of population at $\mathbf{Q}^{\mathrm{mex,OH}}_{1,2}$.

Further insight into the topography of these conical intersections is given in Figs. 5 and 6 which report the energy of states, I^2A and J^2A in the g–h plane as a function of (ρ,θ), for $\mathbf{Q}^{\mathrm{mex,OH}}_{1,2}$ and $\mathbf{Q}^{\mathrm{mex}}_{2,3}$ respectively. First note that from Eq. (1a) the eigenvalues, in this model, are linear functions of ρ. This linearity is evident in Figs. 5a and 6a which report the ρ-dependence for fixed values of θ. The tilt in the cone is a consequence of either $s^{1,2}_x$ or $s^{1,2}_y$ being nonzero. The origin of the name tilt is evident in Fig. 5a, where it is seen that the cone axis is not vertical, that is, the energy at $\theta = 0$ and $\theta = 180$ are not equal for a given ρ. This clearly is a consequence of the nonvanishing $\mathbf{s}^{IJ}$ terms since the term in the radical is unchanged if $\theta \to \theta + \pi$. Thus at $\mathbf{Q}^{\mathrm{mex,OH}}_{1,2}$ the cone is significantly tilted along only the $\mathbf{g}$ direction, since $s^{1,2}_y(\mathbf{Q}^{\mathrm{mex,OH}}_{1,2}) = 0$. This also indicates that at $\mathbf{Q}^{\mathrm{mex,OH}}_{1,2}$ the molecule has C_s symmetry, with the mirror plane perpendicular to the $\hat{\mathbf{y}}$ direction. Note that in Fig. 6b the separation of the eigenvalues is approximately constant while in Fig. 5b it is a dramatic function of θ. This reflects the differences in the asymmetry parameter. When $g^{IJ} \sim h^{IJ}$, the asymmetry is approximately nil, and the energy separation is approximately independent of θ. The derivative coupling, $(1/\rho)/f^{IJ}_\theta$, is a more sensitive indicator of the asymmetry as can also be seen from Figs. 5b and 6b. The θ-dependence of the energy in Fig. 6b is derived from $\mathbf{s}^{IJ}$ and has a sinusoidal dependence. The θ-dependence of the energy in Fig. 5b is derived from a combination of $\mathbf{s}^{IJ}$ and the

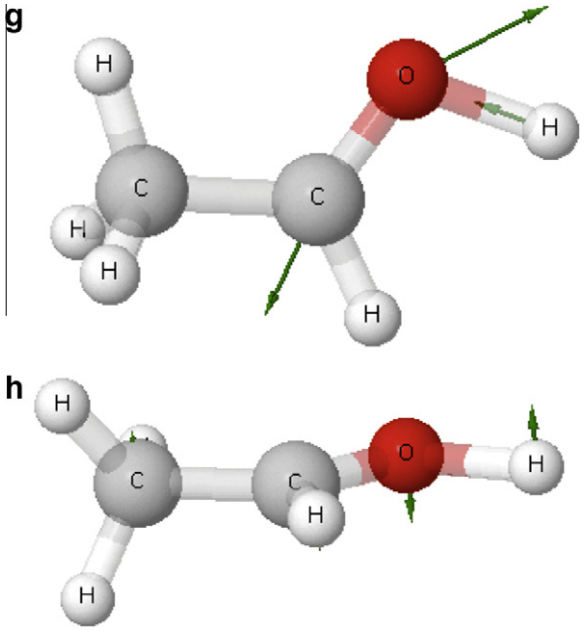

Fig. 2. –**g** and **h** at $\mathbf{Q}^{\mathrm{mex,OH}}_{1,2}$, using "non-methyl" *ras1*.

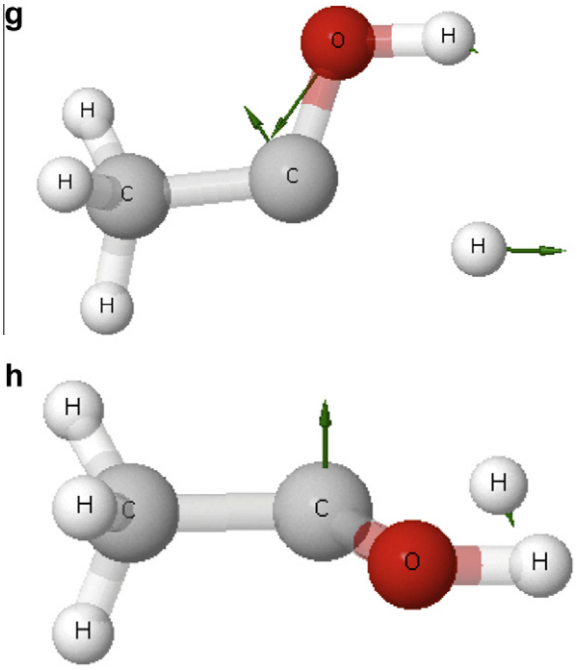

Fig. 3. **g** and **h** at $\mathbf{Q}_{1,2}^{\mathrm{mex,C^{(1)}H^{(2)}}}$, using "non-methyl" *ras1*.

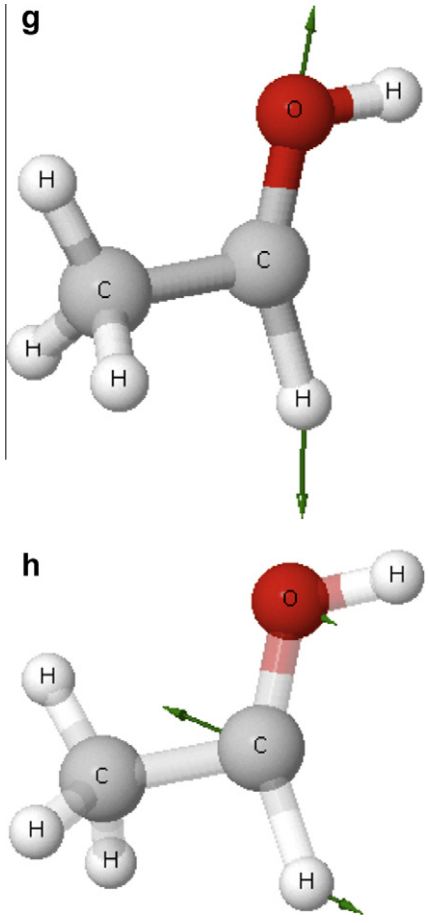

Fig. 4. **g** and **h** at $\mathbf{Q}_{2,3}^{\mathrm{mex}}$, using "non-methyl" *ras1*.

asymmetry, Δ^{IJ}. The implications of these topographies for nuclear dynamics are discussed below.

Table 5
Characteristic parameters at the energy minimized conical intersections, $\mathbf{Q}_{IJ}^{\mathrm{mex,A}}$ "Methyl" case below "non-methyl" case.

I, J, A	g^{IJ}	h^{IJ}	s_x^{IJ}	s_y^{IJ}	Δ^{IJ}	p^{IJ}
1,2,OH	0.18552	0.025639	−0.1061	−0.0004	0.9625	0.1324
	0.18512	0.02209	−0.1044	0.0000	0.9719	0.1318
1,2 $C^{(1)}H^{(2)}$	0.07961	0.05753	0.0715	0.0127	0.3139	0.0695
2,3	0.07320	0.03179	−0.0662	0.0460	0.6826	0.0564
	0.07474	0.03262	−0.0698	0.0428	0.6800	0.0577

3.4. Gradient directed paths

In order to further quantify, in a cost effective manner, the topography in the vicinity of a point **Q** we use gradient directed paths, $\mathbf{l}^j(\mathbf{Q}, S)$, $j = 1, M$, where each j represents a point on a path ($l_k^j(\mathbf{Q}, S)$ is the value of the kth internal coordinate at the jth point) constructed by following the energy gradient starting from the point **Q** on potential energy surface S, with the step size equal to the (scaled) norm of the gradient. Several paths were constructed in this work.

The path, $l^j(\mathbf{Q}_1^{\min}, 2^2\mathrm{A})$, was constructed on the first excited state potential energy surface starting from the Franck–Condon region, that is near $\mathbf{Q}_1^{\min}$ in order to determine the fate of the system after it is photochemically excited to the 3s Rydberg state. This path approaches $\mathbf{Q}_{1,2}^{\mathrm{mex,OH}}$. The path $l^j(\mathbf{Q}_{1,2}^{\mathrm{mex,OH}} - \mathbf{g}^{1,2}(\mathbf{Q}_{1,2}^{\mathrm{mex,OH}}), 1^2\mathrm{A})$ breaks the $OH^{(1)}$ bond, whereas $l^j(\mathbf{Q}_{1,2}^{\mathrm{mex,OH}} + \mathbf{g}^{1,2}(\mathbf{Q}_{1,2}^{\mathrm{mex,OH}}), 1^2\mathrm{A})$ and $l^j(\mathbf{Q}_{1,2}^{\mathrm{mex,OH}} \pm \mathbf{h}^{1,2}(\mathbf{Q}_{1,2}^{\mathrm{mex,OH}}), 1^2\mathrm{A})$ go to $\mathbf{Q}_1^{\min}$. Also $l^j(\mathbf{Q}_{2,3}^{\mathrm{mex}} + \mathbf{h}^{1,2}(\mathbf{Q}_{2,3}^{\mathrm{mex}}), 2^2\mathrm{A})$ takes the system near to $\mathbf{Q}_{1,2}^{\mathrm{mex,OH}}$, whereas $l^j(\mathbf{Q}_{2,3}^{\mathrm{mex}} + \mathbf{g}^{1,2}(\mathbf{Q}_{2,3}^{\mathrm{mex}}), 2^2\mathrm{A})$ takes near to $\mathbf{Q}_{1,2}^{\mathrm{mex,CH}}$.

3.5. Discussion

3.5.1. Comparison of 1-hydroxyethyl and hydroxymethyl

1-Hydroxyethyl can be obtained from hydroxymethyl by the replacement of a hydrogen bound to a carbon by a methyl group. The effect of this methyl substitution on the ground state of the neutral and the cation has been discussed by Krylov and coworkers [24]. See also Ref. [37]. Here we focused on the $2^2\mathrm{A}$ and $3^2\mathrm{A}$ excited states and the $1^2\mathrm{A}$–$2^2\mathrm{A}$, $2^2\mathrm{A}$–$3^2\mathrm{A}$ conical intersections that couple the $2^2\mathrm{A}$ state to the ground state and the $3^2\mathrm{A}$ state to the $2^2\mathrm{A}$ state. The –CH(OH) portion of the equilibrium structures denoted $\mathbf{Q}_1^{\min}$ and $\mathbf{Q}_3^{\min}$ of both CH_3–CH(OH) and H–CH(OH) are quite similar. The same observation holds for the key minimum energy conical intersection points $\mathbf{Q}_{1,2}^{\mathrm{mex,OH}}$ and $\mathbf{Q}_{2,3}^{\mathrm{mex}}$. The $\mathbf{g}^{IJ}$ and $\mathbf{h}^{IJ}$ vectors at $\mathbf{Q}_{1,2}^{\mathrm{mex,OH}}$ and $\mathbf{Q}_{2,3}^{\mathrm{mex}}$ are largely localized on the –CH(OH) portion of these molecules. In each molecule $\mathbf{Q}_2^{\min}$ is absent owing to the conical intersection at $\mathbf{Q}_{1,2}^{\mathrm{mex,OH}}$. Further in each molecule $\mathbf{Q}_{2,3}^{\mathrm{mex}}$ is approximately 0.5 eV above $\mathbf{Q}_3^{\min}$.

3.5.2. Spectra of 1-hydroxyethyl

The above results provide insights into the spectra of 1-hydroxyethyl reported by KEWR and discussed in the Introduction. We begin with the first excited state, the nominal 3s-Rydberg state. The fact that $l^j(\mathbf{Q}_1^{\min}, 2^2\mathrm{A}) \rightarrow \mathbf{Q}_{1,2}^{\mathrm{mex,OH}}$ suggests that nonadiabatic dynamics following excitation to the $2^2\mathrm{A}$ state is governed by the dynamics near $\mathbf{Q}_{1,2}^{\mathrm{mex,OH}}$, although it is germane to note that the "vertical" excitation is predicted at 29,516 cm^{-1}, much higher in energy than the lowest observed electronic excitation. [24] Indeed the absorption onset observed by KEWR at 19,600 ± 100 cm^{-1} is quite close to $E_2(\mathbf{Q}_{1,2}^{\mathrm{mex,OH}})$ implying absorption from the tail of the vibrational wave function. Figs. 2 and 5a and b and Tables 2–4, address the mechanism of photodissociation involving the conical intersection at $\mathbf{Q}_{1,2}^{\mathrm{mex,OH}}$. From Tables 2 and 3 it is seen that motion from $\mathbf{Q}_1^{\min}$ to $\mathbf{Q}_{1,2}^{\mathrm{mex,OH}}$ serves to increase $R_{\mathrm{OH}^{(1)}}$ and decrease $R_{\mathrm{C}^{(1)}\mathrm{O}}$. As seen from Figs. 2 and 5a this motion will tend

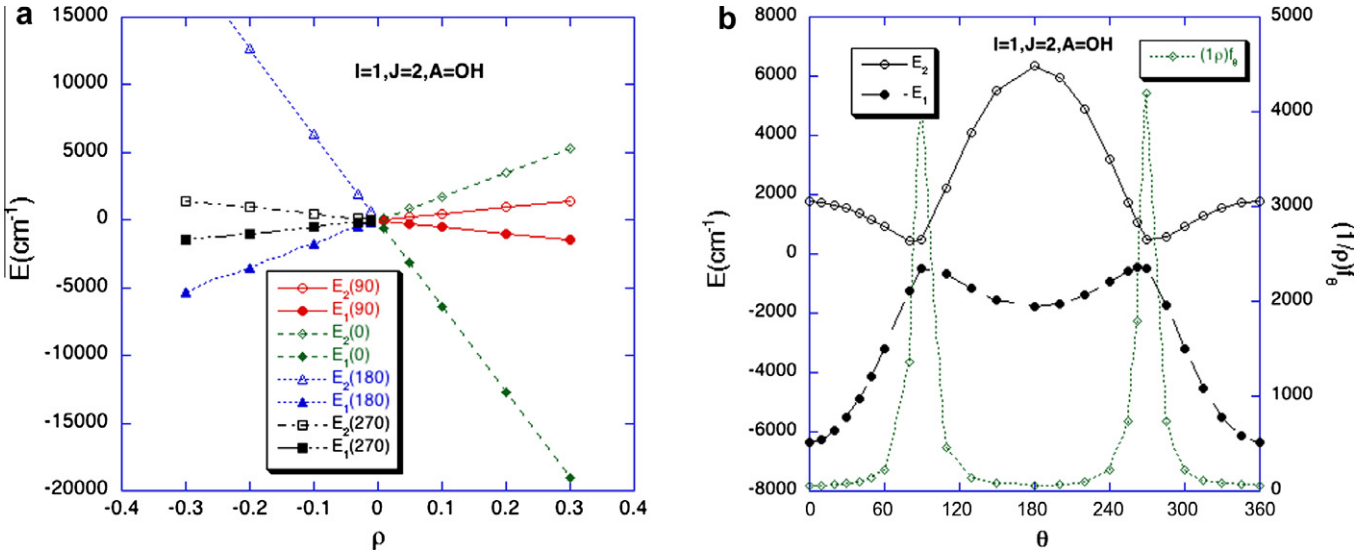

Fig. 5. Energies of the 1^2A and 2^2A states in the vicinity of $\mathbf{Q}_{1,2}^{mex,OH}$ based on the characteristic parameters in Table 5. Plate (a) shows energies as a function of the polar coordinate ρ. For $\theta \geqslant 180° - \rho$ is used. For Plate (b) shows energies a function of θ for $\rho = 0.1$.

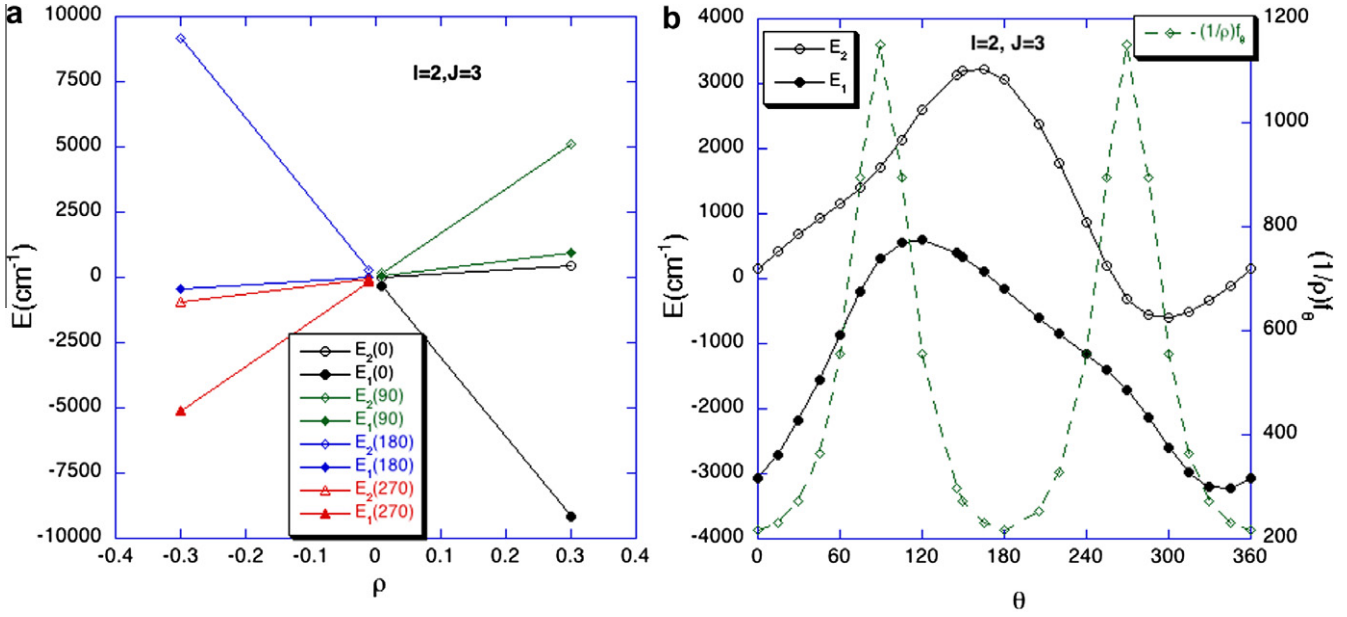

Fig. 6. Energies of the 1^2A and 2^2A states in the vicinity of $\mathbf{Q}_{2,3}^{mex}$ based on the characteristic parameters in Table 5. Plate (a) shows energies as a function of the polar coordinate ρ. For $\theta \geqslant 180° - \rho$ is used. Plate (b) shows energies a function of θ for $\rho = 0.1$.

to move the system through the region of the conical intersection in the direction of increasing $\mathbf{g}^{1,2}$ ($\mathbf{Q}_{1,2}^{mex,OH}$) (open triangles to filled diamonds in Fig. 5a). On the upper potential energy surface as the wave packet approaches the conical intersection (from the left since $R_{OH^{(1)}}$ is increasing) it is routed toward $\theta = 270$ facilitating, since the derivative coupling is large (see Fig. 5b), the nonadiabatic transition to the ground state. The wave packet will emerge in the region near $\theta = 90°$, since the θ increases by 180° passing through the conical intersection. Once on the ground state potential energy surface the preferred path is the $\theta = 0$ direction, that is, increasing $\mathbf{g}^{1.2}$ ($\mathbf{Q}_{1,2}^{mex,OH}$). This preference for the $\theta = 0$ direction reflects the tilt of the conical intersection. Recall too, that the derivative coupling, as noted above, increases like $1/\rho$, so that the probability of a nonadiabatic transition near $\theta = 0$ increases as ρ decreases. While the above discussion is no substitute for real nonadiabatic dynamics, it suggests that the combination of initial kinetic energy plus local topography favor motion in the direction of increasing $\mathbf{g}^{1,2}$ ($\mathbf{Q}_{1,2}^{mex,OH}$) which according to the previous gradient directed path analysis leads to direct, highly nonstatistical, dissociation, breaking the OH bond, with internal energy converted into translational energy. Note that wave packets leaving the region of the conical intersection in the $-\mathbf{g}^{I,J}$ ($\mathbf{Q}_{1,2}^{mex,OH}$) or $\pm\mathbf{h}^{I,J}$ ($\mathbf{Q}_{1,2}^{mex,OH}$) directions would be subject to intramolecular energy redistribution, as they would return to the molecular region. As KEWR explain these alternative paths would be expected to produce some CH_2CHOH which is not observed. This description of photodissociation mediated by the conical intersection at $\mathbf{Q}_{1,2}^{mex,OH}$ is consistent with KEWR's analysis of their spectra. In the region of the 3s Rydberg state absorption, where no REMPI signal is observed, KEWR's analysis of their time-of-flight spectra show: no production of CH_2CHOH although it is energetically accessible (see reaction (1b)); most of the excess energy is deposited in translation and; a strong negative recoil

anisotropy $\beta_{3s} = -0.7$. These experimental results were interpreted by KEWR as supporting direct, nonstatistical dissociation.

The situation changes in the spectral range 32,000–38,000 cm^{-1}. KEWR report a REMPI spectrum, with threshold at 32,360 cm^{-1} and including two peaks above threshold, corresponding to a vibrational progression in the CO stretch. From Table 4 excitations to the 3^2A state are predicted to begin at about 30,275 cm^{-1}. A largely CO stretch mode with frequency 1680 cm^{-1} was found for this state, although a similar vibrational mode is expected for each of the 3p Rydberg states. Given the differences in $R_{C^{(1)}O}$ between $\mathbf{Q}_1^{min}$ and $\mathbf{Q}_3^{min}$ in Table 2, the vibrational progression reported by KEWR is quite reasonable. In the time of flight spectrum at 31,250 two peaks are observed, one isotropic $\beta \sim 0$ and one more anisotropic $\beta \sim -0.4$. For this state, the conical intersection at $\mathbf{Q}_{2,3}^{mex}$ becomes energetically accessible at $E_3(\mathbf{Q}_{2,3}^{mex})$ ~4250 cm^{-1} above threshold, which is $E_3(\mathbf{Q}_3^{min})$, excluding zero point effects, which are small. The topography of this conical intersection is described in Fig. 6 and the g–h plane is reported in Fig. 4. The $\mathbf{g}^{2,3}(\mathbf{Q}_{2,3}^{mex})$, Fig. 4, is seen to involve simultaneous stretching of the $C^{(1)}O$ and $C^{(1)}H^{(2)}$ bonds. As seen from Table 5 and Fig. 6(b) the conical intersection is much less asymmetric than that at $\mathbf{Q}_{1,2}^{mex,OH}$. As a consequence both the $\mathbf{g}^{2,3}(\mathbf{Q}_{2,3}^{mex})$ and $\mathbf{h}^{2,3}(\mathbf{Q}_{2,3}^{mex})$ directions are likely to be accessed from this conical intersection, leading to, as noted above, paths through distinct conical intersections to the ground state potential energy surface. Hence at these energies dissociation involving a combination of direct and more statistical like dynamics is expected. These conclusions are basically in accord with the observations of KEWR. The only difference is that we predict the electronic state in question to be the 3^2A state whereas KEWR assign it to the 5^2A (the $3p_z$ Rydberg) state. Possible resolutions of this issue, which will be the subject of future work, are discussed below.

4. Concluding remarks

This work presents an initial study of the low-lying electronic states, the 1^2A–3^2A states of 1-hydroxyethyl [CH_3CHOH] and the conical intersections that couple them. These results are compared with previous results for hydroxymethyl [CH_2OH] and the 1-hydroxyethyl cation. The 2^2A and the 3^2A states are nominally the 3s and lowest 3p Rydberg states of 1–hydroxyethyl, built on the bound 1-hydroxyethyl cation. Our equilibrium structures of the 1^2A and 3^2A states are in good accord with CCSD(T) determinations of the equilibrium geometries of the ground state of the 1-hydroxyethyl radical and its *cation*, respectively. This serves to confirm the characterization of the 3^2A state, as 3p Rydberg state based on the bound 1-hydroxyethyl cation. Interestingly the 2^2A state, nominally a 3s Rydberg state built on the 1-hydroxyethyl cation, is dissociative, despite the fact that the cation is bound. The absence of a bound 2^2A state is attributed to a conical intersection connecting the 1^2A and 2^2A states located at $\mathbf{Q}_{1,2}^{mex,OH}$. A similar situation was found in hydroxymethyl.

Our results for the 1^2A and 2^2A states are also in good accord with recent experimental measurements KEWR, Ref. [10]. KEWR were unable to observe a REMPI transition involving the 2^2A state and indicated conical intersections as the likely cause. We attributed this specifically to the conical intersection of the 1^2A and 2^2A states at $\mathbf{Q}_{1,2}^{mex,OH}$. We further explained how the products and recoil anisotropy of time-of-flight measurements by KEWR, in the spectral region of the 3s Rydberg state, are consistent with dynamics mediated by that conical intersection.

The lowest energy conical intersection involving the 3^2A and the 2^2A state is ~4200 cm^{-1} above the 3^2A state minimum energy structure. This observation suggests that the low-lying vibrational levels of this state should be visible in REMPI spectroscopy. The analogous levels in CH_2OH were indeed observed by REMPI spectroscopy [14]. However KEWR report no REMPI signal in the spectral region where they expect the 3^2A state. One possible explanation is strong indirect predissociation. In indirect predissociation, coupling of nominally bound vibrational levels of the 3^2A state to the dissociated 2^2A state through the derivative couplings destabilizes the vibrational levels of the 3^2A state on the time scale of the REMPI experiments, without coupling from an accessible conical intersection. The reassignment of the observed spectra should also be considered.

The differences in the observed spectra for hydroxymethyl and 1-hydroxyethyl, in the region of the 3p-Rydberg states raise questions of general interest, concerning the stability of vibration levels in regions where nonadiabatic effects are expected. The competition between indirect and conical intersection induced dissociation merit further study. It is hoped that the results of the present investigation will motivate further studies of nonadiabatic effects in this molecule.

Acknowledgements

This work was funded by Department of Energy Basic Energy Sciences Grant DE-FG02-91ER14189 to DRY. This work is dedicated to Professor Horst Köppel on the occasion of his 60th birthday.

Appendix A. Supplementary data

Supplementary data associated with this article can be found, in the online version, at doi:10.1016/j.chemphys.2010.10.011.

References

[1] S.M. Wu, J.J. Lin, Y.T. Lee, X. Yang, J. Chem. Phys. 111 (1999) 1793.
[2] S. Harich, J.J. Lin, Y.T. Lee, X. Yang, J. Chem. Phys. 111 (1999) 5.
[3] A.H.H. Chang, D.W. Hwang, X.M. Yang, A.M. Mebel, S.H. Lin, Y.T. Lee, J. Chem. Phys. 110 (1999) 10810.
[4] J.J. Lin, S. Harich, Y.T. Lee, X. Yang, J. Chem. Phys. 110 (1999) 10821.
[5] J.J. Lin, C.C. Wang, Y.T. Lee, X.M. Yang, J. Chem. Phys. 113 (2000) 9668.
[6] J.I. Shu, J.J. Lin, Y.T. Lee, X.M. Yang, J. Chem. Phys. 113 (2000) 9678.
[7] J.J. Lin, J. Shu, Y.T. Lee, X. Yang, J. Chem. Phys. 113 (2000) 5287.
[8] C.A. Taatjes, N. Hansen, A. McIlroy, J.A. Miller, J.P. Senosiain, S.J. Klippenstein, F. Qi, L.S. Sheng, Y.W. Zhang, T.A. Cool, J. Wang, P.R. Westmoreland, M.E. Law, T. Kasper, K. Kohse-Hoinghaus, Science 308 (2005) 1887.
[9] H. Choi, R.T. Bise, D.M. Neumark, J. Phys. Chem. A 104 (45) (2000) 10112.
[10] B. Karpichev, L. Edwards, J. Wei, H. Reisler, J. Phys. Chem. A 112 (2008) 412.
[11] C.S. Dulcey, J.W. Hudgens, J. Chem. Phys. 84 (1986). 5262.
[12] L. Feng, A.V. Demyanenko, H. Reisler, J. Chem. Phys. 120 (2004) 6524.
[13] L. Feng, A.V. Demyanenko, H. Reisler, J. Chem. Phys. 118 (2003) 9623.
[14] L. Feng, X. Huang, H. Reisler, J. Chem. Phys. 117 (2002) 4820.
[15] L. Feng, H. Reisler, J. Phys. Chem. A 108 (2004) 7903.
[16] D. Conroy, V. Aristov, L. Feng, H. Reisler, J. Phys. Chem. A 104 (2000) 10288.
[17] F. Chen, E.R. Davidson, J. Phys. Chem. A 105 (2001) 4558.
[18] P.J. Bruna, F. Grein, J. Phys. Chem. A 102 (1998) 3141.
[19] S. Saebø, L. Radom, H.F. Schaefer III, J. Chem. Phys 78 (1983) 845.
[20] B.C. Hoffman, D.R. Yarkony, J. Chem. Phys. 116 (2002) 8300.
[21] A.V. Marenich, J.E. Boggs, J. Chem. Phys. 119 (2003) 10105.
[22] D.R. Yarkony, J. Chem. Phys. 122 (2005) 084316.
[23] P.J. Bruna, F. Grein, J. Phys. Chem. A 105 (2001) 8599.
[24] B. Karpichev, H. Reisler, A.I. Krylov, K. Diri, J. Phys. Chem. A 112 (2008) 9965.
[25] R.D. Johnson, J.W. Hudgens, J. Phys. Chem. 100 (1996) 19874.
[26] J.P. Senosiain, S.J. Klippenstein, J.A. Miller, J. Phys. Chem. A 110 (2006) 6960.
[27] L.A. Curtiss, D.J. Lucas, J.A. Pople, J. Chem. Phys. 102 (1995) 3292.
[28] H. Lischka, M. Dallos, P. Szalay, D.R. Yarkony, R. Shepard, J. Chem. Phys. 120 (2004) 7322.
[29] M. Dallos, H. Lischka, P. Szalay, R. Shepard, D.R. Yarkony, J. Chem. Phys. 120 (2004) 7330.
[30] H. Lischka, R. Shepard, I. Shavitt, R. Pitzer, M. Dallos, T. Müller, P.G. Szalay, F.B. Brown, R. Alhrichs, H.J. Böhm, A. Chang, D.C. Comeau, R. Gdanitz, H. Dachsel, C. Erhard, M. Ernzerhof, P. Höchtl, S. Irle, G. Kedziora, T. Kovar, V. Parasuk, M. Pepper, P. Scharf, H. Schiffer, M. Schindler, M. Schüler, J.-G. Zhao, COLUMBUS, An ab initio Electronic Structure Program, 2003.
[31] T.H. Dunning, J. Chem. Phys. 90 (1989) 1007.
[32] R.D. Bardo, K. Ruedenberg, J. Chem. Phys. 59 (1973) 5956.
[33] T.H. Dunning, J. Chem. Phys. 53 (1970) 2823.
[34] See Supplemental Material.
[35] D.R. Yarkony, J. Chem. Phys. 114 (2001) 2601.
[36] D.R. Yarkony, J. Phys. Chem. A 101 (1997) 4263.
[37] H. Reisler, A.I. Krylov, Int. Rev. Phys. Chem. 28 (2009) 267.